Journal of Applied Physics

RESEARCH ARTICLE | FEBRUARY 21 2023

Measurement of the activation volume in magnetic random access memory

Moosung Choi ; Robert Carpenter ; Maxwel Gama Monteiro ; Simon Van Beek ; Jongryoul Kim ; Sebastien Couet

Journal of Applied Physics 133, 073901 (2023)
https://doi.org/10.1063/5.0135948

Journal of Applied Physics METHOD scitation.org/journal/jap

Measurement of the activation volume in magnetic random access memory

Cite as: J. Appl. Phys. 133, 073901 (2023); doi: 10.1063/5.0135948
Submitted: 23 November 2022 · Accepted: 3 February 2023 ·
Published Online: 21 February 2023

Moosung Choi,[1,2,a)] Robert Carpenter,[3,b)] Maxwel Gama Monteiro,[3] Simon Van Beek,[3] Jongryoul Kim,[1] and Sebastien Couet[3]

AFFILIATIONS

[1]Department of Materials Science and Chemical Engineering, Hanyang University, 15588 Ansan, Republic of Korea
[2]Korea Electric Power Research Institute, 34056 Daejeon, Republic of Korea
[3]imec, Kapeldreef 75, Leuven 3001, Belgium

[a)]**Electronic mail:** kistill1003@gmail.com
[b)]**Author to whom correspondence should be addressed:** robert.carpenter@imec.be

ABSTRACT

Measuring thermal stability in magnetic random access memory devices is non-trivial. Recently, there has been much discussion on the appropriate model to use: single domain or domain wall nucleation. Of particular challenge is assessing the maximum size at which the single domain model can be assumed. Typically, this is estimated to be in the range of 20–30 nm based on a value of the exchange stiffness (A_{ex}) that is assumed, estimated using indirect measurements or derived from significantly thicker films. In this work, it is proposed that this maximum size can be measured directly via the "activation volume" (V_{act}) or the "activation diameter" (D_{act}), which originates from the concept of magnetic viscosity. This is conducted by measuring, using the time dependence of magnetization at different applied fields, D_{act} in perpendicular magnetic tunnel junction pillars of varying effective anisotropy constant (K_{eff}) and diameter. It is shown that the trend in D_{act} follows $\sqrt{1/K_{eff}}$ dependence, in good agreement with the analytic model for the critical diameter of coherent switching. Critically, it is also found that the smallest size for which a single domain, with coherent reversal, occurs is 20 nm. Thus, in devices with technologically relevant values of K_{eff}, the macrospin model may only be used in 20 nm, or smaller, devices.

I. INTRODUCTION

Spin-transfer torque magnetic random access memory (STT-MRAM), consisting of a perpendicular magnetic tunnel junction (p-MTJ), has attracted significant attention for next generation memory. This is due to its non-volatility, fast response speed, high endurance, energy efficiency, scalability, and compatibility with metal–oxide–semiconductor (CMOS) technology. Recently, STT-MRAM has entered mass production for use as an embedded "e-flash" memory.[1,2] In order to expand the applications of STT-MRAM, an increase in the areal density and/or retention time is required. However, the measurement, and modeling, of this is one of the greatest challenges in the development and manufacturing of STT-MRAM.

In magnetic storage, the retention is described by the thermal stability factor, $\Delta = E_b/(k_B T_{Kelvin})$, where E_b is the energy barrier to reversal, k_B is Boltzmann's constant, and T is the absolute temperature. The calculation of E_b is dependent on the reversal mechanism of the magnetic entity, in this case the free layer (FL). The simplest case is that described by the "macrospin model" where there is coherent reversal of a single domain magnetic entity with uniaxial anisotropy. Thus, at $\mu_0 H = 0$ mT, $E_b = K_{eff} V$, where V is the magnetic volume of the FL and K_{eff} is the effective anisotropy constant.[29] It is important to note at this point that, even in this regime, the reality is that the switching process is likely to not be "quasi-coherent." Instead, it will likely follow a mechanism more in line with "curling" or "fanning";[3] however, this discussion is beyond the scope of this work.

The other reversal mechanism commonly used is described by that of domain wall nucleation where $E_b = w\sigma$, where $\sigma = 4\sqrt{A_{ex} K_{eff} t_{FL}}$ is the domain wall energy density with A_{ex}, t_{FL} is the exchange stiffness, and FL is the thickness, respectively. The wall surface area, $w = t_{FL} D_{MTJ}$, is given by t_{FL} and the MTJ device

diameter D_{MTJ}.[4,5] Therefore, the calculated value of E_b, and trend with respect to D_{MTJ} or t_{FL}, can vary significantly depending on the model selected.

The transition between the single domain and domain wall nucleation mechanisms is dependent on the competition between the magnetostatic and anisotropy energies. In MTJ devices, the value of K_{eff} is calculated, typically using the values measured in non-patterned films, as will be discussed later. However, the measurement of A_{ex}, which is required for the domain wall energy, is non-trivial. This ranges from the estimation in trends of Δ,[6,7] in comparison with micromagnetic or atomistic models[5,8–11] and, recently, the temperature dependence of magnetization.[12] This inaccuracy in A_{ex}, therefore, makes it challenging to accurately estimate the maximum device, or cell, size in which a single domain can be assumed.

In this work, it is postulated that this maximum size can be directly measured through that of the activation volume (V_{act}). This is demonstrated in p-MTJ arrays for pillars 20 and 60 nm in diameter with varying free layer thicknesses. Using this measurement, the selection of the correct model and/or cell size for modeling of Δ can be made.

II. METHOD

A. Sample preparation

The free layer (FL) structure used in this work was MgO/$Co_{17.5}Fe_{52.5}B_{30}(t_x)$/Ta(0.4)/$Co_{17.5}Fe_{52.5}B_{30}(t_y)$/MgO (nm), where the first and last MgO layers are the tunnel barrier, and a cap used to provide an additional interfacial anisotropy, respectively. The role of the spacer layer is as a B getter and is sufficiently thin for direct coupling, as described in previous works.[13,14] In the case of this work, the range of t_{FL} studied was 1.9–2.6 nm, where the value is a summation of the two CoFeB thicknesses, t_x and t_y, as defined above. Finally, the reference layer (RL) structure consisted of a CoFeB and Co/Pt based synthetic antiferromagnet (SAF) multi-layer. The deposition of the p-MTJ films was carried out by magnetron sputtering (Canon-Avelva EC7800) on 300 mm, thermally oxidized, Si wafers. The thicknesses of all the layers was controlled through calibration of the deposition rates, which, depending on the deposition conditions, are in the range of 0.1–1 Å/s. To simulate back end of line thermal budget conditions, the films were post-annealed at 400°C in a vacuum environment for 30 min (TEL-MS2 MRT5000). These films were then patterned into large arrays of pillars with diameters of 20 or 60 nm, with a center to center separation of 50 and 200 nm, respectively. These arrays were printed using extreme UV (20 nm diameter, 50 nm pitch) and immersion (60 nm diameter, 200 nm pitch) lithography, followed by patterning via ion beam etching. A schematic of the magnetic structure, a summary of the samples, and example scanning electron microscope images of the 60 and 20 nm pillars are shown in Figs. 1(a)–1(c), respectively.

B. Theory of measurement

In the study of thermally activated reversal over the energy barrier, coupling of the thermal energy and magnetic moment is mathematically not possible. Néel postulated that the thermal energy could be represented as a "thermal fluctuation field" (H_f) defined as $H_f = k_B T_{Kelvin}/Q$, where Q was an undefined parameter.[15] It was Wohlfarth[16] that gave a definition of Q arguing on dimensional grounds to give the equation

$$H_f = (k_B T_{Kelvin})/(V_{act} M_s). \quad (1)$$

Wohlfarth described V_{act} as an "activation volume" for the nucleation of a single domain reversal for a particle or region of a continuous film. This gives V_{act} as the maximum size at which a magnetic entity can reverse as a single domain particle in a single thermal activation process.[16,17] The value of V_{act} was originally

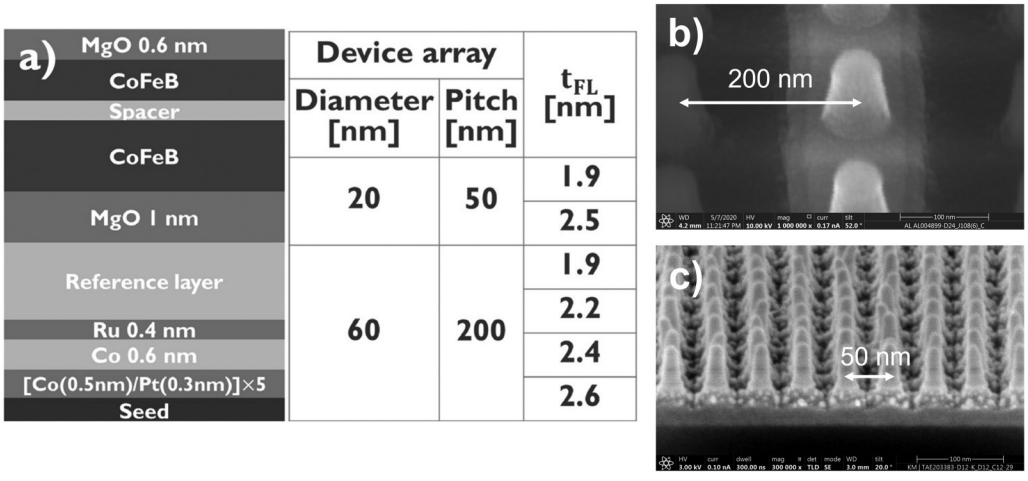

FIG. 1. (a) Schematic of the p-MTJ multi-layer, details of the patterned structures, and cross-section scanning electron microscope image showing (b) 60 and (c) 20 nm devices.

calculated using the measurement of the irreversible susceptibility (χ_{irr}) and the slope of the time dependence of magnetization [$S(H)$]. This has been demonstrated in a number of systems from a single domain[18,19] to coupled granular.[20,21] However, in the case of p-MTJ devices, the value of χ_{irr} cannot be measured accurately due to the large demagnetizing field (H_d). Furthermore, a non-linear dependence of $S(H)$ in $ln(t)$ is expected in systems with a narrow distribution of K_{eff} and size, such as expected in that of p-MTJ devices. Thus, the classical techniques cannot be used. In the work of El Hilo *et al.*,[22] this is accounted for in an equation of state analysis giving a measurement of the form

$$H_f = \left.\frac{\delta H}{\delta \ln(t)}\right|_M, \tag{2}$$

where the value of H_f is determined via a waiting-time measurement. This is given as the slope in $\ln(t)$ of the time (t_1/t_2) taken by the magnetization to fall to a fixed value, M, under different applied fields (H_1/H_2) separated by an increment δH. This is measured around the coercivity (H_c) of the system to set $M = 0$ so that the average value of $H_d = 0$. Such a measurement has been demonstrated in perpendicular recording media[23] and will be extended to p-MTJ systems in this work.

C. Measurement procedure

The waiting-time measurements in this work were carried out using a magneto-optical Kerr effect (MOKE) magnetometer in a polar configuration (Microsense PKMRAM). The spot size of the laser is 1 mm, covering approximately $\sim 25 \times 10^6$ and $\sim 400 \times 10^6$ pillars for the 60 and 20 nm device arrays, respectively. The position of the laser spot, with respect to the pillar arrays, is shown schematically in Fig. 2 (inset). A further description of the system

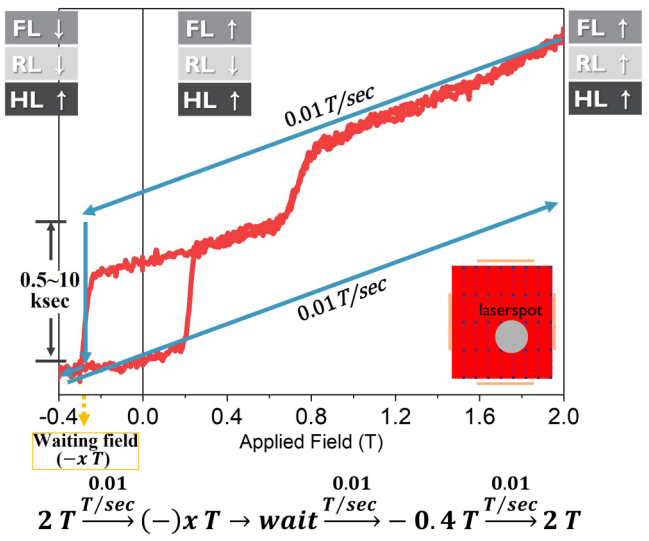

FIG. 2. Figure showing the field sweep procedure, with measure location on the pillar array inset.

configuration and measurement sequence is covered in previous works.[13] An example of the measurement sequence is shown in Fig. 2. At the initial state, all magnetic layers (free/reference/hard layers) are aligned parallelly. The field is then reduced to a waiting field ($-x$) with a constant ramp rate of 0.01 T/s in order to limit sweep rate dependent effects. While the waiting field was held, the change in the Kerr signal was measured for fixed times ranging from 0.5×10^3 to 10×10^3 s depending on that required for the system to reach $M = 0$. After this time, a field of -0.4 T was applied to fully reverse the FL. Only the FL was reversed to negative saturation so that the local dipolar fields would not be altered by any reversal of the reference (RL) or hard (HL) layers. This measurement sequence was repeated for a minimum of eight waiting fields per sample condition. The waiting fields were selected between the start of the reversal process to the FL coercivity ($-H_c$).

The values of the saturation magnetization (M_s) and anisotropy field (H_K) were measured using a vibrating sample magnetometer (VSM) (Microsense EZ11) on non-patterned samples. With M_s and H_f, it is possible to calculate V_{act} using Eq. (1).

III. RESULTS AND DISCUSSION

The procedure for extracting H_f from the waiting-time measurements is shown in Fig. 3. In Fig. 3(a), the change in M/M_s with H_{ext} is shown, where the step due to the waiting-time can be seen with respect to min/max saturation. It is important to note that the abrupt, linear changes in M/M_s do not imply instantaneous reversal but is due to the time dependent measurement at a constant applied field. The time dependence of M/M_s with respect to the waiting fields is shown in Fig. 3(b). This behavior is due to the thermal fluctuation after effect as described earlier. The large noise in the measurement at longer time scales is due to the high sampling rate used ($\sim$0.1 s) with respect to the signal to noise ratio. The crossing at $M/M_s = 0$ was taken from the moving average. These times to reach $M/M_s = 0$ for the different fields are plotted with respect to $\ln(t)$ as shown in Fig. 3(c). The quality of the data, despite the noise seen in Fig. 3(b), is evident from the linear fit. As shown in Eq. (2) and Refs. 22 and 23, the slope of this fit directly gives the value of H_f. This measurement was repeated five times for each of the 60 nm arrays to measure repeatability. The relative standard deviation obtained for each value of $\mu_0 H_f$ was less than 2%, further verifying the quality of the data.

Table I shows the magnetic properties obtained from the VSM measurements of the non-patterned films with respect to t_{FL}, alongside the associated values of $\mu_0 H_f$ measured in the patterned structures. The value of M_s was extracted from the linear relationship of $M_s \times t_{FL}$ with t_{FL}, as shown in Fig. 4. The magnetic dead layer (t_d) due to the Ta spacer is calculated from the y-intercept as shown in Ref. 24. From these measurements, it is found that $M_s = 1.178$ MA/m and $t_d = 0.54$ nm, in good agreement with that expected for Ta/CoFeB systems.[24] The effective anisotropy field, H_K, of the FL is measured, following the Stoner–Wohlfarth model,[16] from the hard axis saturation field. The RL/HL contributions are removed through comparison to a reference sample where the FL signal is not present. These measured values are shown in Table I. The effective perpendicular magnetic anisotropy (PMA) energy per unit area of the FL, $K_{eff} \times t_{eff,FL}$, can then be calculated

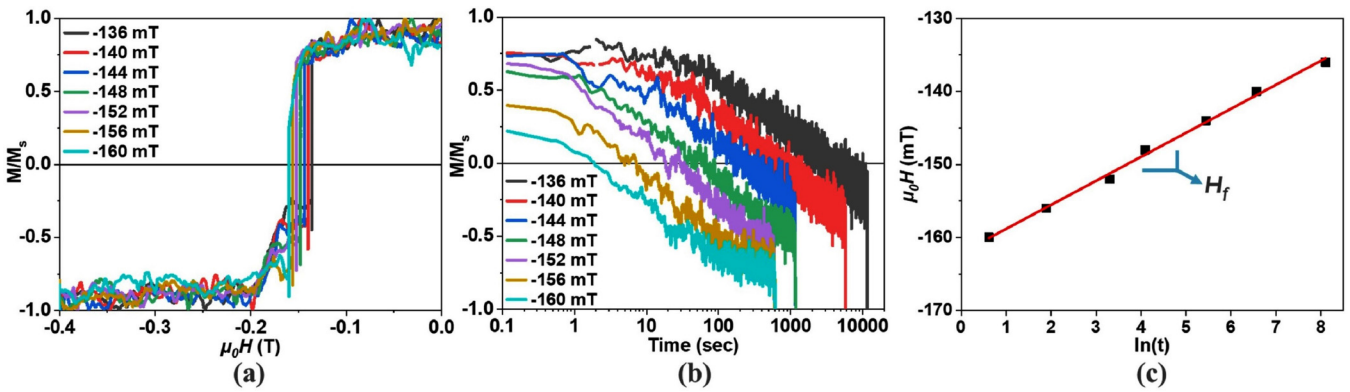

FIG. 3. Analysis process for the waiting-time measurement of 60 nm pillars with $t_{FL} = 2.4$ nm: (a) M/M_s vs $\mu_0 H$, (b) M/M_s vs t, and (c) the reversal field dependence in ln(t).

using Eq. (3), where $t_{eff,FL} = t_{FL} - t_d$,

$$K_{eff} t_{eff,FL} = \frac{\mu_0 M_s H_K t_{eff,FL}}{2}, \tag{3}$$

where the values of $K_{eff} t_{eff,FL}$ obtained are in the range of 0.2–0.7 mJ/m^2, in good agreement with previous studies.[14] It is important to note that the Stoner–Wohlfarth model assumes $T_{Kelvin} = 0°$ K, whereas these measurements were all carried out at $T_{Kelvin} = 300°$ K. This will lead to a deviation in the FL magnetization vector of $5 - 15°$, depending on local defects, from the easy axis. This will give an error in the measured value of H_K up to 30%.[16,17] This error is taken into account for all measurements related to H_K.

Using the measured M_s and H_f values, the activation volume of the MTJ arrays can be calculated using Eq. (1). In this study, the activation diameter (D_{act}) will be used instead of V_{act}. This is calculated under the assumption that the area corresponding to the activation volume has a cylindrical body $V_{act} = \pi(D_{act}/2)^2 t_{eff,FL}$, as in the case of a p-MTJ device. Due to the large anisotropy and thin FL, it is unlikely that a domain wall can form horizontally; thus, this assumption is reasonable.

Figure 5 shows the measured D_{act}, and corresponding H_f, values with respect to t_{FL}. It is found that D_{act} (H_f) increases (decreases) with t_{FL}. For the 60 nm D_{MTJ} pillars, D_{act} is smaller for all values of t_{FL} showing that in these sizes, there should only be incoherent, or domain wall, reversal. For the 20 nm D_{MTJ} pillars, D_{act} is limited to that of the physical size. One interpretation is that when D_{MTJ} is smaller than D_{act}, this should then be defined by the physical dimensions. This is the case where the single domain regime can be assumed. This is similar to the studies of V_{act} vs grain size with respect to intergranular coupling shown in recording media.[21,23] Indeed, this is expected to be the case; however, a change in the D_{MTJ} may also cause a change in K_{eff} of the pillar. Thus, this must also be taken into account.

In order to calculate K_{eff} in the patterned films, the different anisotropy components are required. In the non-patterned films, K_{eff} and its components can be defined as

TABLE I. Measured magnetic properties of the non-patterned films with the associated values of H_f.

t_{FL} (nm)	$M_s t_{FL}$ (mA)	$\mu_0 H_K$ (mT)	$K_{eff} t_{eff,FL}$ (mJ/m^2)	$t_{eff,FL}$ (nm)	$\mu_0 H_f$ (mT)
1.9	1.6 ± 0.008	878 ± 7	0.71 ± 0.009	1.4	8.0
2.1	1.8 ± 0.002	659 ± 3	0.60 ± 0.003	1.5	9.8
2.2	2.0 ± 0.004	466 ± 3	0.47 ± 0.004	1.7	5.9
2.4	2.1 ± 0.007	257 ± 5	0.27 ± 0.006	1.8	3.2
2.5	2.3 ± 0.004	175 ± 5	0.20 ± 0.006	2.0	4.4

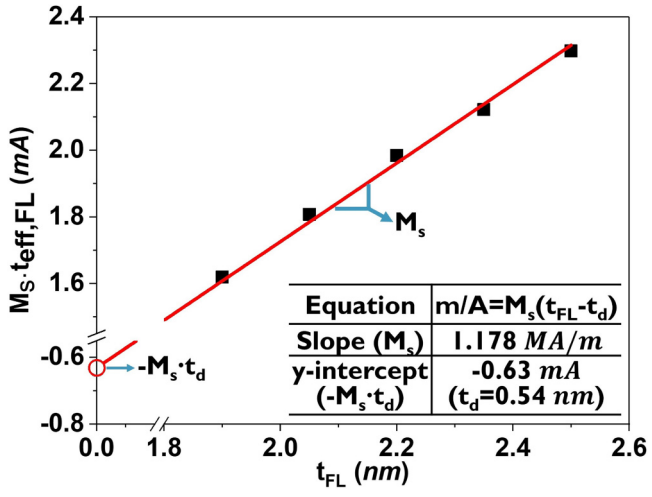

FIG. 4. Graph showing the measurement of M_s from the slope of $M_s \times t_{FL}$ with respect to t_{FL}.

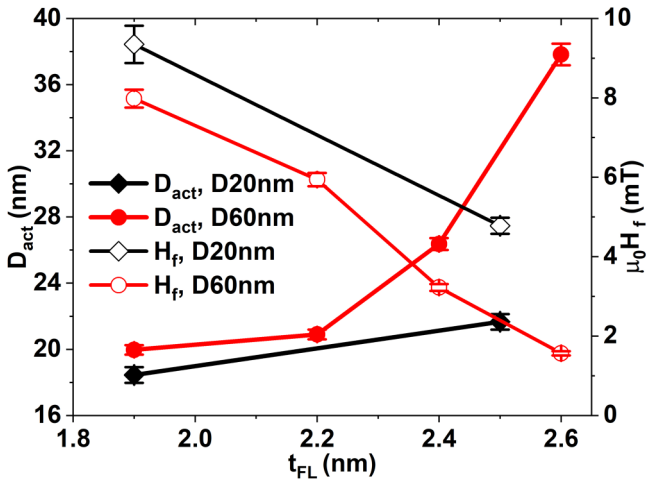

FIG. 5. The change in D_{act} and H_c of the patterned devices with respect to t_{FL} and device size.

$$K_{eff} = -\frac{1}{2}\mu_0 M_s^2 + \frac{K_i}{t_{eff,FL}}, \tag{4}$$

where a positive (negative) value gives an out-of-plane (in-plane) preferred orientation. The $-\mu_0 M_s^2/2$ term is the definition of shape anisotropy in an infinite thin film. The second term is the interfacial anisotropy constant (K_i) of the CoFeB/MgO interface. Here, the magneto-crystalline anisotropy term is neglected as it is cubic and, thus, will contribute equally in/out of plane. The values of K_{eff} obtained for the non-patterned films, for all values of t_{FL} used, are found to be greater than 1×10^5 J/m^3, as expected from an MgO/CoFeB system.[25] The dependence of K_{eff} with $t_{eff,FL}$ is shown in Fig. 6. Fitting this dependence with Eq. (4), using the values of M_s obtained previously (see Table I), gives $K_i = 1.902 \times 10^{-3}$ J/m^2.

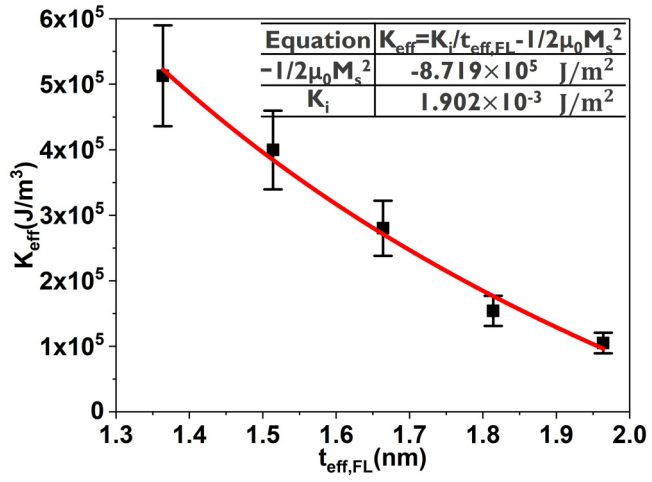

FIG. 6. Graph showing the calculation of K_i from the fit of Eq. (4) using the measured values from Table I.

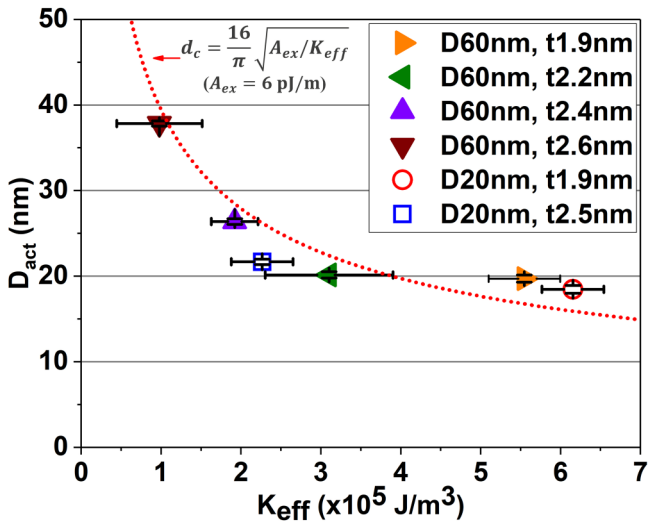

FIG. 7. The relationship between the measured D_{act} and calculated K_{eff} in the patterned devices where the dotted line is a fit of d_c as defined in Eq. (6) using a value of $A_{ex} = 6$ pJ/m.

In the patterned film, Eq. (4) takes the form

$$K_{eff} = -\frac{1}{2}\mu_0 M_s^2 (N_z - N_x) + \frac{K_i}{t_{eff,FL}}. \tag{5}$$

Here, the shape anisotropy term is defined as that of a cylinder where N_x and N_z are the out-of-plane and in-plane demagnetization factors, respectively. N_x and N_z were calculated using Sato's formula for a cylinder.[26] The M_s and K_i values are assumed to be intrinsic to the CoFeB/MgO system and, thus, are kept equal in both the non-patterned and patterned films.

Figure 7 shows the trend of the measured D_{act} with respect to the value of K_{eff} calculated from Eq. (5) for the patterned devices. The data follow a $\sqrt{1/K_{eff}}$ dependence, regardless of the pillar diameter. This is in excellent agreement with the analytical model for the critical diameter, d_c at which the transition from macrospin to domain wall reversal occurs,[8,11] as given by

$$d_c = \frac{16}{\pi}\sqrt{\frac{A_{ex}}{K_{eff}}}. \tag{6}$$

If the data are fit with Eq. (6), a value of $A_{ex} \equiv 6$ pJ/m is obtained in excellent agreement with recent works.[5,12,28] This result shows that the value of D_{act}, thus, reflects that of the maximum size at which single domain behavior occurs. Furthermore, this shows that for p-MTJs within this range of K_{eff} and M_s, the device/cell size for which the macrospin model can be used is 20–40 nm. Of particular note, D_{act} saturates at 20 nm for $K_{eff} > 2.5 \times 10^5$

J/m^3. This shows that, for industrially relevant anisotropies, a macrospin model should only be used for devices with a diameter <20 nm. In addition to providing a clear regime for the selection of model to use for the calculation of Δ, this technique provides a direct measurement of H_f. In theory, this could be linked to the thermal exchange length λ_{thex}.[27] However, this is beyond the scope of the current study and so will be explored in future works.

IV. CONCLUSION

In this study, the measurement of H_f via field accelerated thermal activation using a waiting-time technique was demonstrated on patterned p-MTJ arrays. By using measurements of the magnetic properties obtained from the non-patterned films, D_{act} was calculated. By comparing different FL thicknesses and device sizes, the dependence of D_{act} with respect to K_{eff} was measured and found to follow a trend of $\sqrt{1/K_{eff}}$, which is similar to that of d_c, the analytical description for the diameter at which the transition from macrospin to domain wall reversal occurs.[8,11] This shows that D_{act} can be considered equivalent to the maximum size at which single domain reversal will occur, which, for the samples in this work, was found to be between 20 and 40 nm depending on the value K_{eff}. This shows that this technique can be used to measure, in patterned devices, the cell/pillar size at which single domain behavior can be assumed, thus giving a clear indication of whether the macrospin or domain wall model is relevant for the given system.

ACKNOWLEDGMENTS

This research was supported by the MOTIE (Ministry of Trade, Industry, and Energy) in Korea, under the Fostering Global Talents for Innovative Growth Program (P0008745) supervised by the Korea Institute for Advancement of Technology (KIAT) and imec's Industrial Affiliation Program on STT-MRAM devices. In addition, all the authors would like to acknowledge the support of imec's fab, line, and hardware teams. Last but not least, R. Carpenter would like to thank Professor Kevin O'Grady for fruitful discussions on the underlying theory of reversal mechanisms in polycrystalline thin films.

AUTHOR DECLARATIONS

Conflict of Interest

The authors have no conflicts to disclose.

Author Contributions

Moosung Choi: Investigation (equal); Methodology (lead); Writing – original draft (equal); Writing – review & editing (equal). **Robert Carpenter:** Conceptualization (lead); Investigation (equal); Methodology (supporting); Supervision (lead); Writing – original draft (equal); Writing – review & editing (equal). **Maxwel Gama Monteiro:** Formal analysis (supporting); Validation (supporting). **Simon Van Beek:** Methodology (supporting); Writing – review & editing (supporting). **Jongryoul Kim:** Resources (equal); Supervision (equal). **Sebastien Couet:** Project administration (supporting); Resources (lead); Supervision (supporting).

DATA AVAILABILITY

The data that support the findings of this study are available from the corresponding author upon reasonable request.

REFERENCES

[1]K. Lee, J. H. Bak, Y. J. Kim, C. K. Kim, A. Antonyan, D. H. Chang, S. H. Hwang, G. W. Lee, N. Y. Ji, W. J. Kim, J. H. Lee, B. J. Bae, J. H. Park, I. H. Kim, B. Y. Seo, S. H. Han, Y. Ji, H. T. Jung, S. I. Park, O. I. Kwon, J. W. Kye, Y. D. Kim, S. W. Pae, Y. J. Song, G. T. Jeong, K. H. Hwang, G. H. HKoh, H. K. Kang, and E. S. Jung, "1Gbit high density embedded STT-MRAM in 28 nm FDSOI technology," in *IEDM* (IEEE, 2019), pp. 19–23.
[2]Y. Ji, H. Goo, J. Lim, T. Y. Jeong, T. Uemura, G. R. Kim, B. I. Seo, S. Lee, G. Park, J. Jo, S. I. Han, K. Lee, J. Lee, S. H. Hwang, D. S. Lee, S. Pyo, H. T. Jung, S. H. Han, S. Noh, K. Suh, S. Y. Yoon, H. Nam, H. Hwang, H. Jiang, J. W. Kim, D. Kwon, Y. J. Song, K. H. Koh, H. S. Rhee, S. Pae, and E. Lee, "Reliability of industrial grade embedded-STT-MRAM," in *IRPS* (IEEE, 2020).
[3]B. D. Cullity and C. D. Graham, *Introduction to Magnetic Materials* (IEEE Press/Wiley, 2009).
[4]R. Skomski, *Simple Models of Magnetism* (Oxford University Press, 2008).
[5]C. Yoshida, T. Tanaka, T. Ataka, J. Fujisaki, K. Shimizu, T. Hirahara, H. Shitara, A. Furuya, and Y. Uehara, "Size dependence of the thermal stability factor in a perpendicular CoFeB/MgO magnetic tunnel junction studied by micromagnetic simulations," Jpn. J. Appl. Phys. **58**, SBBB05 (2019).
[6]H. Sato, M. Yamanouchi, K. Miura, S. Ikeda, R. Koizumi, F. Matsukura, and H. Ohno, "CoFeB thickness dependence of thermal stability factor in CoFeB/MgO perpendicular magnetic tunnel junctions," IEEE Magn. Lett. **3**, 3000204 (2012).
[7]H. Sato, E. C. I. Enobio, M. Yamanouchi, S. Ikeda, S. Fukami, S. Kanai, F. Matsukura, and H. Ohno, "Properties of magnetic tunnel junctions with a MgO/CoFeB/Ta/CoFeB/MgO recording structure down to junction diameter of 11 nm," Appl. Phys. Lett. **105**, 062403 (2014).
[8]G. D. Chaves-O'Flynn, G. Wolf, J. Z. Sun, and A. D. Kent, "Thermal stability of magnetic states in circular thin-film nanomagnets with large perpendicular magnetic anisotropy," Phys. Rev. Appl. **4**, 024010 (2015).
[9]I. Volvach, J. G. Alzate, Y.-J. Chen, A. J. Smith, D. L. Kencke, and V. Lomakin, "Thermal stability and magnetization switching in perpendicular magnetic tunnel junctions," Appl. Phys. Lett. **116**, 192408 (2020).
[10]A. Meo, R. Chepulskyy, D. Apalkov, R. W. Chantrell, and R. F. L. Evans, "Atomistic investigation of the temperature and size dependence of the energy barrier of CoFeB/MgO nanodots," J. Appl. Phys. **128**, 073905 (2020).
[11]J. Z. Sun, R. P. Robertazzi, J. Nowak, P. L. Trouilloud, G. Hu, D. W. Abraham, M. C. Gaidis, S. L. Brown, E. J. O'Sullivan, W. J. Gallagher, and D. C. Worledge, "Effect of subvolume excitation and spin-torque efficiency on magnetic switching," Phys. Rev. B **84**, 064413 (2011).
[12]J. B. Mohammadi, B. Kardasz, G. Wolf, Y. Chen, M. Pinarbasi, and A. D. Kent, "Reduced exchange interactions in magnetic tunnel junction free layers with insertion layers," ACS Appl. Electron. Mater. **1**, 10 (2019).
[13]S. Van Beek, R. Carpenter, S. Kundu, S. Couet, J. Swerts, and G. Sankar Kar, "The magneto-optical Kerr effect for efficient characterization of thermal stability in dense arrays of p-MTJs," AIP Adv. **9**, 125236 (2019).
[14]S. Couet, T. Devolder, J. Swerts, S. Mertens, T. Lin, E. Liu, S. Van Elshocht, and G. Sankar Kar, "Impact of Ta and W-based spacers in double MgO STT-MRAM free layers on perpendicular anisotropy and damping," Appl. Phys. Lett. **111**, 152406 (2017).
[15]L. Néel, "Théorie du traînage magnétique des ferromagnétiques en grains fins avec application aux terres cuites," Ann. Geophys. **5**, 99–136 (1949).
[16]E. P. Wohlfarth, "The coefficient of magnetic viscosity," J. Phys. F: Met. Phys. **14**, L155–L159 (1984).
[17]K. O'Grady, private communication (2022).
[18]P. Gaunt, "Magnetic viscosity and thermal activation energy," J. Appl. Phys. **59**, 4129 (1986).

[19]A. M. de Witte and K. O'Grady, "The activation volumes of reversal in ultra-fine particles and recording media," IEEE Trans. Mag. **26**, 1810 (1990).
[20]I. S. Jacobs and C. P. Bean, "An approach to elongated fine-particle magnets," Phys. Rev. **100**, 1060–1067 (1955).
[21]Y. Inaba, T. Shimatsu, H. Muraoka, J. D. Dutson, and K. O'Grady, "Activation volumes in CoPtCr-SiO_2 perpendicular recording media," IEEE Trans. Mag. **41**, 3130–3132 (2005).
[22]M. El-Hilo, K. O'Grady, and R. W. Chantrell, "Fluctuation fields and reversal mechanisms in granular magnetic systems," J. Magn. Magn. Mater. **248**, 360–373 (2002).
[23]J. Chureemart, L. Lauri, T. P. Nolan, and K. O'Grady, "The effect of SiO_2 content on activation volumes in exchange coupled composite media," J. Appl. Phys. **114**, 083907 (2013).
[24]Y.-H. Wang, W.-C. Chen, S.-Y. Yang, K.-H. Shen, C. Park, M.-J. Kao, and M.-J. Tsai, "Interfacial and annealing effects on magnetic properties of CoFeB thin films," J. Appl. Phys. **99**, 08M307 (2006).
[25]M. Wang, Y. Zhang, X. Zhao, and W. Zhao, "Tunnel junction with perpendicular magnetic anisotropy: Status and challenges," Micromachines **6**, 1023–1045 (2015).
[26]M. Sato and Y. Ishii, "Simple and approximate expressions of demagnetizing factors of uniformly magnetized rectangular rod and cylinder," J. Appl. Phys. **66**, 983–985 (1989).
[27]M. Hahn, "Temperature in micromagnetism: Cell size and scaling effects of the stochastic Landau–Lifshitz equation," J. Phys. Commun. **3**, 075009 (2019).
[28]G. Mihajlović, N. Smith, T. Santos, J. Li, B. D. Terris, and J. A. Katine, "Thermal stability for domain wall mediated magnetization reversal in perpendicular STT MRAM cells with W insertion layers," Appl. Phys. Lett. **117**, 242404 (2020).
[29]E. C. Stoner and E. P. Wohlfarth, "A mechanism of magnetic hysteresis in heterogeneous alloys," Philos. Trans. R. Soc. A **240**, 599–642 (1948).